DOI: 10.1021/ic101033n

Inorganic Chemistry
Article

Metal Monophosphonates $M\{(2\text{-}C_5H_4NO)CH_2PO_3\}(H_2O)_2$ (M = Co, Ni, Mn, Cd): Synthesis, Structure, and Magnetism

Ting-Hai Yang,[†] Elisabeth S. Knowles,[‡] Daniel M. Pajerowski,[‡] Jian-Sheng Xia,[‡] Liang Yin,[‡] Song Gao,[§] Mark W. Meisel,*[,‡] and Li-Min Zheng*[,†]

[†]*State Key Laboratory of Coordination Chemistry, School of Chemistry and Chemical Engineering, Nanjing University, Nanjing 210093, People's Republic of China,* [‡]*Department of Physics and the National High Magnetic Field Laboratory, University of Florida, Gainesville, Florida 32611-8440, and* [§]*Beijing National Laboratory for Molecular Sciences, College of Chemistry and Molecular Engineering, Peking University, Beijing 100871, People's Republic of China*

Received May 21, 2010

Four isostructural metal monophosphonates, $M\{(2\text{-}C_5H_4NO)CH_2PO_3\}(H_2O)_2$ with M = Co (**1**), Ni (**2**), Mn (**3**), and Cd (**4**), were synthesized and structurally characterized. These compounds show a double-chain structure in which the $M_2(\mu\text{-}O)_2$ dimers are connected by O−P−O bridges. The magnetic responses of **1**−**3** were investigated over a wide range of magnetic fields (up to 10 T) and temperatures (down to 50 mK). Except for **4**, which is weakly diamagnetic from 2 K to room temperature, the dominant magnetic interactions are antiferromagnetic. Isothermal magnetic field sweeps at 50 mK provide signatures in the magnetic responses that are associated with antiferromagnetic to field-induced fully polarized (magnetically saturated) transitions. Analysis of the magnetic data indicates that **1** and **2** form magnetic dimer-like clusters with weak dimer−dimer interactions present. Contrastingly, the magnetic interactions present in **3** are significantly weaker, so a definitive description of the magnetism of this compound is elusive.

Introduction

The interdisciplinary field of materials chemistry necessarily interfaces with several research fields that possess different motivations. For example, new materials with novel properties may possess potential applications in the fields of catalysis, electronics, and medicine, and for these reasons, metallic coordination complexes have received prodigious attention. In parallel, spatially low-dimensional arrangements, i.e., chains, ladders, and planes, of magnetic spins may exhibit responses that can be modeled theoretically and numerically.[1] The research described herein is an example of a fusion of these apparently disparate directions of research. Specifically, metal phosphonate chemistry has an extensive history,[2] while simultaneously, isostructural, low-dimensional model systems that simply possess a tuning of the magnetic spin value S have not been identified in a set of real materials but have been the focus of wide-ranging theoretical and numerical work.[3] It is important to stress that the underlying structural architecture does not necessarily reveal the underlying network of magnetic interactions, and in the field of magnetic spin ladders, this naive extrapolation has[4−7] and has not[8−10] been realized.

*To whom correspondence should be addressed. E-mail: lmzheng@nju.edu.cn (L.-M.Z.), meisel@phys.ufl.edu (M.W.M.). Fax: +86-25-83314502 (L.-M.Z.), 1-352-392-3591 (M.W.M.).

(1) (a) Dagotto, E.; Rice, T. M. *Science* **1996**, *271*, 618. (b) Sachdev, S. *Science* **2000**, *288*, 475. (c) Wang, X.; Yu, L. *Phys. Rev. Lett.* **2000**, *84*, 5399. (d) Sachdev, S. *Nat. Phys.* **2008**, *4*, 173. (e) Giamarchi, T.; Rüegg, Ch.; Tchernyshyov, O. *Nat. Phys.* **2008**, *4*, 198. (f) Xu, C.; Sachdev, S. *Phys. Rev. B* **2009**, *79*, 064405.

(2) (a) Thompson, M. E. *Chem. Mater.* **1994**, *6*, 1168. (b) Clearfield, A. *Curr. Opin. Solid State Mater. Sci.* **1996**, *1*, 268. (c) Clearfield, A. *Curr. Opin. Solid State Mater. Sci.* **2002**, *6*, 495.

(3) (a) Schulz, H. J. *Phys. Rev. B* **1986**, *34*, 6372. (b) Kim, Y. J.; Greven, M.; Wiese, U.-J.; Birgeneau, R. J. *Eur. Phys. J. B* **1998**, *4*, 291. (c) Chen, S.; Wu, C.; Zhang, S.-C.; Wang, Y. *Phys. Rev. B* **2005**, *72*, 214428. (d) Assis, P. E. G.; Libero, V. L.; Capelle, K. *Phys. Rev. B* **2005**, *71*, 052402. (e) Almeida, J.; Martin-Delgado, M. A.; Sierra, G. *J. Phys. A: Math. Theor.* **2008**, *41*, 485301.

(4) (a) Azuma, M.; Hiroi, Z.; Takano, M.; Ishida, K.; Kitaoka, Y. *Phys. Rev. Lett.* **1994**, *73*, 3463. (b) Uehara, M.; Nagata, T.; Akimitsu, J.; Takahashi, H. T.; Mori, N.; Kinoshita, K. *J. Phys. Soc. Jpn.* **1996**, *65*, 2764.

(5) (a) Landee, C. P.; Turnbull, M. M.; Galeriu, C.; Giantsidis, J.; Woodward, F. M. *Phys. Rev. B* **2001**, *63*, 100402. (b) Shapiro, A.; Landee, C. P.; Turnbull, M. M.; Jornet, J.; Deumal, M.; Novoa, J. J.; Robb, M. A.; Lewis, W. *J. Am. Chem. Soc.* **2007**, *129*, 952.

(6) (a) Patyal, B. R.; Scott, B. L.; Willett, R. D. *Phys. Rev. B* **1990**, *41*, 1657. (b) Watson, B. C.; Kotov, V. N.; Meisel, M. W.; Hall, D. W.; Granroth, G. E.; Montfrooij, W. T.; Nagler, S. E.; Jensen, D. A.; Backov, R.; Petruska, M. A.; Fanucci, G. E.; Talham, D. R. *Phys. Rev. Lett.* **2001**, *86*, 5168. (c) Lorenz, T.; Heyer, O.; Garst, M.; Anfuso, F.; Rosch, A.; Rüegg, Ch.; Krämer, K. *Phys. Rev. Lett.* **2008**, *100*, 067208. (d) Klanjšek, M.; Mayaffre, H.; Berthier, C.; Horvatić, M.; Chiari, B.; Piovesana, O.; Bouillot, P.; Kollath, C.; Orignac, E.; Citro, R.; Giamarchi, T. *Phys. Rev. Lett.* **2008**, *101*, 137207. (e) Rüegg, Ch.; Kiefer, K.; Thielemann, B.; McMorrow, D. F.; Zapf, V.; Normand, B.; Zvonarev, M. B.; Bouillot, P.; Kollath, C.; Giamarchi, T.; Capponi, S.; Poilblanc, D.; Biner, D.; Krämer, K. W. *Phys. Rev. Lett.* **2008**, *101*, 247202.

(7) Ribas, X.; Mas-Torrent, M.; Perez-Benitez, A.; Dias, J. C.; Alves, H.; Lopes, E. B.; Henriques, R. T.; Molins, E.; Santos, I. C.; Wurst, K.; Foury-Leylekian, P.; Almeida, M.; Veciana, J.; Rovira, C. *Adv. Funct. Mater.* **2005**, *15*, 1023.

(8) (a) Johnston, D. C.; Johnson, J. W.; Goshorn, D. P.; Jacobson, A. J. *Phys. Rev. B* **1987**, *35*, 219. (b) Garrett, A. W.; Nagler, S. E.; Tennant, D. A.; Sales, B. C.; Barnes, T. *Phys. Rev. Lett.* **1997**, *79*, 745.

Published on Web 08/24/2010

Previously, by using 1-hydroxyethylidenediphosphonate [hedp; $CH_3C(OH)(PO_3)_2$], a subset of the present authors synthesized a series of compounds containing $\{M_2(hedpH)_2\}_n^{2n-}$ double-chain structures.[11] Herein, we present a new synthetic approach by reacting a monophosphonic acid, e.g., (2-pyridyl *N*-oxide)methylphosphonic acid [2-pompH$_2$; (2-C_5H_4NO)-$CH_2PO_3H_2$] with metal salts under hydrothermal conditions. Four new nearly isostructural compounds, M{(2-C_5H_4NO)-CH_2PO_3}$(H_2O)_2$ [M = Co^{II} (**1**), Ni^{II} (**2**), Mn^{II} (**3**), Cd^{II} (**4**)], with double-chain structures have been obtained. In other words, on the basis of the structure alone, we conjectured that these compounds might be antiferromagnetic spin ladders whose magnetic responses were simply tuned by the differences in the spin value *S*, albeit with some subtle variations of the nearest-neighbor (*nn*) magnetic superexchange *J*. Magnetic measurements made with standard commercial magnetometers capable of spanning a range of temperature, *T*, and magnetic field, *B*, parameter space, namely, 2 K $\leq T \leq$ 300 K and $0 \leq B \leq 7$ T, suggested that **1**−**3** possess antiferromagnetic *nn* interactions and field-induced transitions at low temperatures. Consequently, the magnetic studies were extended to low temperatures, $T \geq 50$ mK, and to high magnetic fields, $B \leq 10$ T, which allowed the antiferromagnetic to fully spin-polarized transition to be identified. Analysis of the magnetic data reveals that the strongest magnetic interactions generate spin dimers, which have varying degrees of coupling to neighboring dimers.

Experimental Section

Materials and Methods. 2-(Pyridyl *N*-oxide)methylphosphonic acid was prepared according to the literature.[12] All of the other starting materials were obtained from commercial sources and were used without further purification. Elemental analyses were performed on a PE240C elemental analyzer. The IR spectra were recorded on a Vector 22 FT-IR spectrometer with pressed KBr pellets. Thermal analyses were performed in nitrogen in the temperature range 20−800 °C with a heating rate of 10 °C/min on a TGA-DTA V101B TA Instrument 2100. The powder X-ray diffraction (XRD) patterns were recorded on a Shimadzu XD-3A X-ray diffractometer. Variable-temperature magnetic susceptibility data were obtained on polycrystalline samples using a Quantum Design MPMS-XL5 SQUID magnetometer in Nanjing and a MPMS-XL7 in Gainesville. Diamagnetic contributions were estimated from Pascal's constants.[13] The low-temperature (down to 50 mK), high-magnetic-field (up to 10 T) studies employed alternating-current (ac) mutual inductance coils mounted on a dilution refrigerator. The arrangement, which is described elsewhere[14] and in the Supporting Information (SI), allowed a sample, nominally 25 mg, to be immersed in pure ^{3}He, which provided intimate thermal contact with the mixing chamber of the dilution refrigerator. Various frequencies, ranging from 24.7 to 555 Hz, were used to search for an optimal response, and the ac field was nominally 0.1 mT. Typically, the data were obtained by isothermal field sweeps of 50 mT/min, which avoided heating and provided reversible results, except for the case of **3**, as will be described later. A detailed discussion of the data is given in the SI.

Synthesis of Co{(2-C_5H_4NO)CH_2PO_3}$(H_2O)_2$ (1). A mixture of $Co(OAc)_2 \cdot 6H_2O$ (0.2 mmol, 0.049 g) and 2-pompH$_2$ (0.2 mmol, 0.038 g) in 8 mL of H_2O was kept in a Teflon-lined autoclave at 140 °C for 48 h. After slow cooling to room temperature, purple-red needlelike crystals were collected as a single phase, judging by the powder XRD measurement. Yield: 32 mg (57%). Anal. Found (calcd) for $C_6H_{10}NO_6PCo$: C, 25.51 (25.55); H, 3.59 (3.57); N, 4.93 (4.97). IR (KBr, cm^{-1}): 3406 m, 3263 m, 2943 m, 1615 w, 1571 w, 1494 m, 1442 m, 1402 w, 1306 w, 1221 s, 1204 w, 1143 w, 1110 s, 1080 w, 1059 s, 967 s, 869 m, 826 w, 803 w, 780 m, 703 m, 619 w, 583 m, 563 m, 527 w, 496 w, 473 w, 438 w. Thermal analysis showed a weight loss of 13.4% in the 160−280 °C temperature range, close to the calculated value for the release of two H_2O molecules (12.8%).

Synthesis of Ni{(2-C_5H_4NO)CH_2PO_3}$(H_2O)_2$ (2). A mixture of $Ni(OAc)_2 \cdot 6H_2O$ (0.1 mmol, 0.025 g) and 2-pompH$_2$ (0.1 mmol, 0.019 g) in 8 mL of H_2O was kept in a Teflon-lined autoclave at 140 °C for 48 h. After slow cooling to room temperature, the light-green needlelike crystals were collected as a single phase, judging by the powder XRD measurement. Yield: 17 mg (61%). Anal. Found (calcd) for $C_6H_{10}NO_6PNi$: C, 25.42 (25.58); H, 3.59 (3.58); N, 4.93 (4.97). IR (KBr, cm^{-1}): 3386 m, 3263 m, 2946 m, 1615 w, 1571 w, 1494 m, 1443 m, 1401 w, 1308 w, 1222 s, 1203 w, 1143 w, 1112 s, 1056 s, 970 s, 926 w, 870 m, 806 w, 782 m, 704 m, 619 w, 586 m, 566 m, 533 w, 496 w, 476 w, 439 w. Thermal analysis showed a weight loss of 12.6% in the 160−280 °C temperature range, close to the calculated value for the release of two H_2O molecules (12.8%).

Synthesis of Mn{(2-C_5H_4NO)CH_2PO_3}$(H_2O)_2$ (3). A mixture of $Mn(OAc)_2$ (0.2 mmol, 0.049 g) and 2-pompH$_2$ (0.2 mmol, 0.038 g) in 8 mL of H_2O was kept in a Teflon-lined autoclave at 140 °C for 48 h. After slow cooling to room temperature, light-yellow blocklike crystals were collected as a single phase, judging by the powder XRD measurement. Yield: 41 mg (74%). Anal. Found (calcd) for $C_6H_{10}NO_6PMn$: C, 25.93 (25.92); H, 3.69 (3.62); N, 5.20 (5.04). IR (KBr, cm^{-1}): 3405 m, 3242 m, 2937 m, 1613 w, 1568 w, 1493 m, 1439 m, 1403 w, 1303 w, 1223 s, 1206 w, 1143 w, 1109 s, 1082 w, 1063 s, 973 s, 926 w, 869 m, 826 w, 802 w, 781 m, 701 m, 619 w, 580 m, 560 m, 520 w, 494 w, 471 w, 438 w. Thermal analysis showed a weight loss of 13.1% in the 160−260 °C temperature range, close to the calculated value for the release of two H_2O molecules (13.0%).

Synthesis of Cd{(2-C_5H_4NO)CH_2PO_3}$(H_2O)_2$ (4). A mixture of $CdSO_4 \cdot {}^8/_3H_2O$ (0.2 mmol, 0.051 g) and 2-pompH$_2$ (0.2 mmol, 0.038 g) in 8 mL of H_2O, adjusted to pH = 3.3 with 1 M NaOH, was kept in a Teflon-lined autoclave at 140 °C for 48 h. After slow cooling to room temperature, colorless blocklike crystals were collected as a single phase, judging by the powder XRD measurement. Yield: 27 mg (41%). Anal. Found (calcd) for $C_6H_{10}NO_6PCo$: C, 21.42 (21.48); H, 3.10 (3.00); N, 4.19 (4.17). IR (KBr, cm^{-1}): 3397 m, 3178 m, 2932 m, 1637 w, 1566 w, 1492 m, 1437 m, 1404 w, 1301 w, 1259 w, 1218 s, 1142 w, 1105 s, 1081 w, 1060 s, 974 s, 867 w, 827 w, 796 w, 780 m, 700 m, 618 w, 577 m, 559 m, 520 w, 495 w, 470 w, 439 w. Thermal analysis showed a weight loss of 10.9% in the 140−210 °C temperature range, close to the calculated value for the release of two H_2O molecules (10.7%).

X-ray Crystallographic Analysis. Single crystals of dimensions $0.3 \times 0.2 \times 0.1$ mm^3 for **1**, $0.3 \times 0.18 \times 0.16$ mm^3 for **2**, $0.4 \times 0.3 \times 0.2$ mm^3 for **3**, and $0.4 \times 0.3 \times 0.3$ mm^3 for **4** were selected for indexing and intensity data collection at 298 K on a Bruker SMART APEX CCD diffractometer equipped with graphite-monochromatized Mo Kα (λ = 0.710 73 Å) radiation. A hemisphere of data was

(9) (a) Chiari, B.; Piovesana, O.; Tarantelli, T.; Zanazzi, P. F. *Inorg. Chem.* **1990**, *29*, 1172. (b) Hammar, P. R.; Reich, D. H. *J. Appl. Phys.* **1996**, *79*, 5392. (c) Chaboussant, G.; Crowell, P. A.; Levy, L. P.; Piovesana, O.; Madouri, A.; Mailly, D. *Phys. Rev. B* **1997**, *55*, 3046. (d) Stone, M. B.; Chen, Y.; Rittner, J.; Yardimci, H.; Reich, D. H.; Broholm, C.; Ferraris, D. V.; Lectka, T. *Phys. Rev. B* **2002**, *65*, 064423.

(10) (a) Willett, R. D. *J. Chem. Phys.* **1966**, *44*, 39. (b) Willett, R. D.; Twamley, B.; Montfrooij, W.; Granroth, G. E.; Nagler, S. E.; Hall, D. W.; Park, J.-H.; Watson, B. C.; Meisel, M. W.; Talham, D. R. *Inorg. Chem.* **2006**, *45*, 7689. (c) Stone, M. B.; Tian, W.; Lumsden, M. D.; Granroth, G. E.; Mandrus, D.; Chung, J.-H.; Harrison, N.; Nagler, S. E. *Phys. Rev. Lett.* **2007**, *99*, 087204.

(11) (a) Yin, P.; Gao, S.; Zheng, L.-M.; Xin, X.-Q. *Chem. Mater.* **2003**, *15*, 3233. (b) Yin, P.; Gao, S.; Wang, Z.-M.; Yan, C.-H.; Zheng, L.-M.; Xin, X.-Q. *Inorg. Chem.* **2005**, *44*, 2761. (c) Zhang, Z.-C.; Gao, S.; Zheng, L.-M. *Dalton Trans.* **2007**, 4681. (d) Zhang, Z.-C.; Bao, S.-S.; Zheng, L.-M. *Inorg. Chem. Commun.* **2007**, *10*, 1063.

(12) Gan, X.-M.; Binyamin, I.; Rapko, B. M.; Fox, J.; Duesler, E. N.; Paine, R. T. *Inorg. Chem.* **2003**, *43*, 2443–2448.

(13) Kahn, O. *Molecular Magnetism*; VCH Publishers: New York, 1993.

(14) Orendáčová, A.; Čižmár, E.; Sedláková, L.; Hanko, J.; Kajňaková, M.; Orendáč, M.; Feher, A.; Xia, J. S.; Yin, L.; Pajerowski, D. M.; Meisel, M. W.; Zeleňák, V.; Zvyagin, S.; Wosnitza, J. *Phys. Rev. B* **2009**, *80*, 144418.

Table 1. Crystallographic Data for **1**−**4**

	1	**2**	**3**	**4**
empirical formula	$C_6H_{10}NO_6PCo$	$C_6H_{10}NO_6PNi$	$C_6H_{10}NO_6PMn$	$C_6H_{10}NO_6PCd$
fw	282.05	281.83	278.06	335.52
cryst syst	triclinic	triclinic	triclinic	triclinic
space group	$P\bar{1}$	$P\bar{1}$	$P\bar{1}$	$P\bar{1}$
a (Å)	6.525(3)	6.480(3)	6.629(1)	6.739(2)
b (Å)	7.487(3)	7.416(2)	7.566(2)	7.602(2)
c (Å)	10.005(4)	9.910(2)	10.043(2)	10.067(3)
α (deg)	88.645(7)	88.39(1)	88.847(3)	88.607(4)
β (deg)	78.272(7)	77.98(3)	78.714(3)	78.721(4)
γ (deg)	70.516(8)	70.09(2)	70.543(3)	70.705(4)
V (Å^3)	450.7(3)	437.5(3)	465.2(2)	476.9(3)
Z	2	2	2	2
d_{calcd} (g/cm^3)	2.079	2.140	1.985	2.336
F(000)	286	288	282	328
GOF on F^2	0.876	1.008	1.004	1.030
R1, wR2 [$I > 2\sigma(I)$][a]	0.0673, 0.1022	0.0553, 0.1151	0.0307, 0.0979	0.0285, 0.0914
R1, wR2 (all data)[a]	0.1170, 0.1122	0.0764, 0.1209	0.0323, 0.0993	0.0289, 0.0921
$\Delta\rho_{max}$, $\Delta\rho_{min}$ (e/Å^3)	0.764, −0.925	0.412, −0.792	0.497, −0.509	0.714, −0.891

[a] $R1 = \sum||F_o| - |F_c||/\sum|F_o|$, $wR2 = [\sum w(F_o^2 - F_c^2)^2/\sum w(F_o^2)^2]^{1/2}$.

Table 2. Selected Bond Lengths [Å] and Angles [deg] for **1**−**4**[a]

	1	**2**	**3**	**4**
M1−O1	2.069(6)	2.033(4)	2.108(2)	2.201(3)
M1−O2A	2.114(5)	2.101(4)	2.158(2)	2.252(3)
M1−O2B	2.172(6)	2.141(4)	2.250(2)	2.314(3)
M1−O4	2.079(6)	2.047(4)	2.204(2)	2.320(3)
M1−O1W	2.100(5)	2.027(4)	2.173(2)	2.261(3)
M1−O2W	2.155(6)	2.093(4)	2.239(2)	2.333(3)
P1−O1	1.502(6)	1.493(4)	1.519(2)	1.518(3)
P1−O2	1.525(6)	1.503(4)	1.534(2)	1.527(3)
P1−O3	1.523(5)	1.522(4)	1.511(2)	1.507(3)
N1−O4	1.316(8)	1.347(5)	1.328(3)	1.320(4)
O1−M1−O2A	97.3(2)	95.1(2)	98.4(1)	99.2(1)
O1−M1−O1W	90.0(2)	90.4(2)	90.1(1)	90.7(1)
O2A−M1−O1W	172.0(2)	172.5(2)	170.5(1)	168.0(1)
O1−M1−O4	98.7(2)	97.8(1)	97.5(1)	97.3(1)
O2A−M1−O4	84.7(2)	83.4(2)	84.1(1)	81.9(1)
O1W−M1−O4	90.9(2)	90.8(2)	90.7(1)	90.1(1)
O1−M1−O2W	91.5(2)	91.6(2)	94.1(1)	95.3(1)
O2A−M1−O2W	90.0(2)	90.9(2)	89.1(1)	88.1(1)
O1W−M1−O2W	93.2(2)	94.1(2)	94.5(1)	97.9(1)
O4−M1−O2W	169.0(2)	169.4(2)	167.3(1)	165.0(1)
O1−M1−O2B	175.8(3)	175.9(2)	178.4(1)	178.9(1)
O2A−M1−O2B	81.8(2)	83.2(2)	81.8(1)	81.8(1)
O1W−M1−O2B	91.1(2)	91.7(2)	89.8(1)	88.5(1)
O4−M1−O2B	85.3(2)	85.7(2)	84.1(1)	83.5(1)
O2W−M1−O2B	84.4(2)	84.8(2)	84.4(1)	84.1(1)
M1A−O2−M1C	98.2(2)	96.8(2)	98.2(1)	98.3(1)

[a] Symmetry codes: A, $-x$, $-y$, $-z$; B, $x+1$, y, z; C, $x-1$, y, z.

collected in the θ range 2.08−25.04° for **1**, 2.16−26.00° for **2**, 2.07−25.00° for **3**, and 2.84−25.00° for **4** using a narrow-frame method with a scan width of 0.3° in ω and an exposure time of 5 s per frame. The numbers of measured and observed reflections [$I > 2\sigma(I)$] are 2237 and 1560 (R_{int} = 0.0731) for **1**, 2300 and 1654 (R_{int}= 0.0262) for **2**, 2326 and 1603 (R_{int} = 0.0110) for **3**, and 2303 and 1629 (R_{int} = 0.0164) for **4**, respectively. The data were integrated using the Siemens *SAINT* program.[15] Empirical absorption corrections were applied. The structures were solved by direct methods and refined on F^2 by full-matrix least squares using *SHELXTL*.[16] All of the non-H atoms were refined anisotropically. All H atoms were refined isotropically. Crystallographic and refinement details are listed in Table 1. Selected bond lengths and angles are given in Table 2.

(15) *SANIT, Program for Data Extraction and Reduction*; Siemens Analytical X-ray Instruments: Madison, WI, 1994−1996.

(16) *SHELXTL, Reference Manual*, version 5.0; Siemens Industrial Automation, Analytical Instrumentation: Madison, WI, 1995.

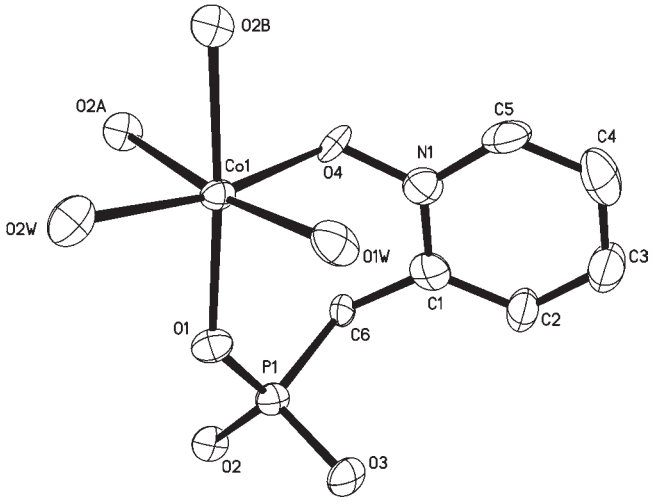

Figure 1. Building unit of **1** with the atomic labeling scheme (50% probability). All H atoms are omitted for clarity.

CCDC 683367, 663368, 683369, and 781787 contain the supplementary crystallographic data for this paper. These data can be obtained free of charge at www.ccdc.cam.ac.uk/conts/retrieving.html [or from the Cambridge Crystallographic Data Centre, 12 Union Road, Cambridge CB2 1EZ, U.K.; fax (int.) +44-1223/336-033; e-mail deposit@ccdc.cam.ac.uk].

Results and Discussion

Crystal Structures. Compounds **1**−**4** are isostructural, crystallizing in a triclinic lattice with space group $P\bar{1}$, so **1** will be discussed as a generic example. The asymmetric unit consists of one Co atom, one 2-pomp^{2-} ligand, and two coordinated H_2O molecules (Figure 1). The Co atom has a distorted octahedral environment, surrounded by three phosphonate O atoms (O1, O2A, and O2B), one pyridyl *N*-oxide (O4), and two H_2O molecules (O1W and O2W). The Co−O bond lengths are in the range 2.069(6)−2.172(6) Å. The 2-pomp^{2-} ligand chelates the Co atom through O1 and O4 atoms and bridges the equivalent Co atoms via O2 to form a double chain along the *a* axis that contains {Co_2-(μ-O)$_2$} dimers (Figure 2). Within the dimer, the Co1A···Co1C distance is 3.239 Å and the Co1A−O−Co1C angle is 98.2(2)°. The Co···Co distances across the O−P−O

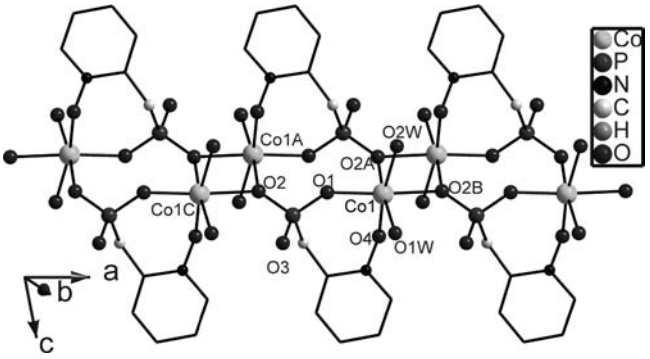

Figure 2. Fragment of the structural chain in compound **1**. All H atoms are omitted for clarity.

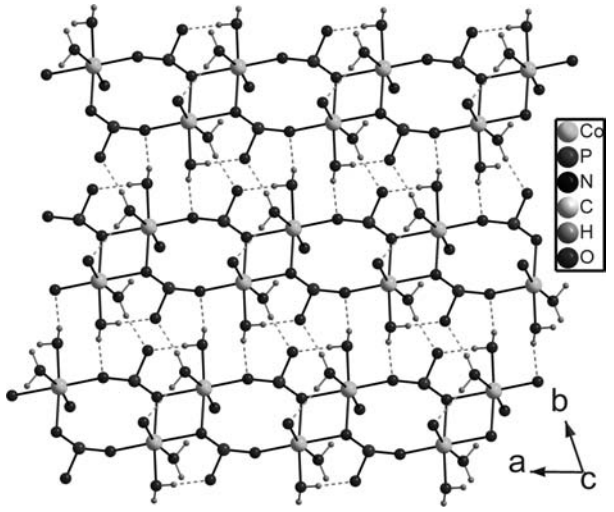

Figure 3. *ab* layer of structure **1**. This layer consists of double chains linked through hydrogen bonds (dashed lines).

bridges are 5.109 Å for Co1···Co1A and 6.525 Å for Co1···Co1C.

Moderately strong hydrogen-bonding interactions are observed between the chains through the pendant phosphonate oxygen O3 [P1−O3 = 1.523(5) Å] and the coordinated H_2O molecules, forming a supramolecular layer in the *ab* plane (Figure 3). The $\pi-\pi$-stacking interaction exists between the pyridyl groups from the adjacent layers (plane−plane distances, 3.005 and 3.330 Å; centroid−centroid distances, 3.430 and 4.386 Å; angles between the ring normal of the pyridyl plane and the centroid vector, 13.7 and 47.0°; Figure 4).[17]

Structures **2**−**4** are identical with **1** except the different metal atoms. The M···M distances across the μ-O(P) bridge are 3.173 Å for **2**, 3.332 Å for **3**, and 3.453 Å for **4**. Those across the O−P−O bridges are 5.116 and 6.480 Å for **2**, 5.161 and 6.629 Å for **3**, and 5.247 and 6.739 Å for **4**. The M−O−M bond angles are 96.8(2)° for **2**, 98.0(1)° for **3**, and 98.2(1)° for **4**.

Clearly, one-dimensional metal phosphonates with double-chain structures can be obtained successfully by using a monophosphonate ligand. A careful analysis reveals that the skeleton of the double chains in **1**−**3** is quite similar to that in the Mhedp chain compounds.[11] Nevertheless, the incorporation of a pyridyl group into a monophosphonate ligand affects not only the structural parameters within the double chain but also the packing of the chains. Compared with the chains in $(NH_3-R-NH_3)M_2(hedpH)_2\cdot xH_2O$ (M = Fe, Co, Mn), the M−O−M bond angles in **1**−**4** (∼96.8−98.2°) are much smaller (∼98.8−103.7° in the former) and the M···M distances over the O−P−O bridges (∼5.1 and 6.5−6.7 Å) are significantly elongated (∼4.8 and 5.5 Å in the former), although those across the μ-O(P) bridge are similar (∼3.3 Å). In addition, the packing modes of the double chains are completely different. In $(NH_3-R-NH_3)M_2(hedpH)_2\cdot xH_2O$, the double chains are connected via strong hydrogen-bonding interactions, while in **1**−**4**, the packing is through moderately strong hydrogen bonds and $\pi-\pi$ stacking of pyridyl groups. Finally, with regard to the paramagnetic systems **1**−**3**, elongation of the M···M distances over the O−P−O bridges might be expected to significantly reduce the magnetic exchange coupling through these pathways.

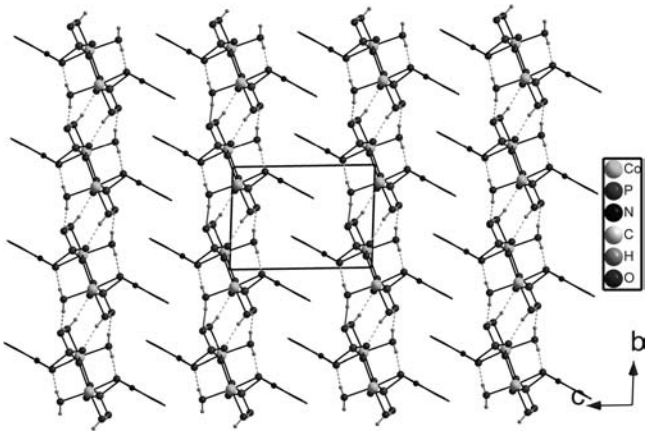

Figure 4. Structure **1** packed along the *a* axis. All H atoms except those in the H_2O molecules are omitted for clarity.

Magnetic Properties: Low Magnetic Field. The low-magnetic-field magnetic responses of **1**−**3** are shown in Figure 5 as the temperature dependence of the direct-current (dc) magnetic susceptibility, $\chi = M/B$, and the product χT, where T is the temperature. As a first attempt, these data can be fit by expressions that assume that the dominant magnetic contributions arise from magnetic spin dimers, originating from the interaction J of *nn* spins $\mathbf{S}_A$ and $\mathbf{S}_B$, whose Hamiltonian can be written as[13]

$$\mathscr{H} = -J\mathbf{S}_A\cdot\mathbf{S}_B \tag{1}$$

such that

$$\chi_{dimer}(T) = \frac{Ng^2\mu_B{}^2}{3k_BT}\,\frac{\sum_{S=0}^{2S_A} S(S+1)(2S+1)\exp\left[\frac{1}{2}S(S+1)\frac{J}{k_BT}\right]}{\sum_{S=0}^{2S_A}(2S+1)\exp\left[\frac{1}{2}S(S+1)\frac{J}{k_BT}\right]} \tag{2}$$

where N is Avagrado's number, g is the Landé g factor, μ_B is the Bohr magneton, k_B is Boltzmann's constant, and here S is the spin of the dimer state. This simplified approach did not adequately reproduce the data, so the mean-field description of weak interdimer interactions, J', weighted by the magnetic coordination number z, was included along with a Curie description of possible unpaired spins, ρ, and

(17) Janiak, C. *J. Chem. Soc., Dalton Trans.* **2000**, 3885.

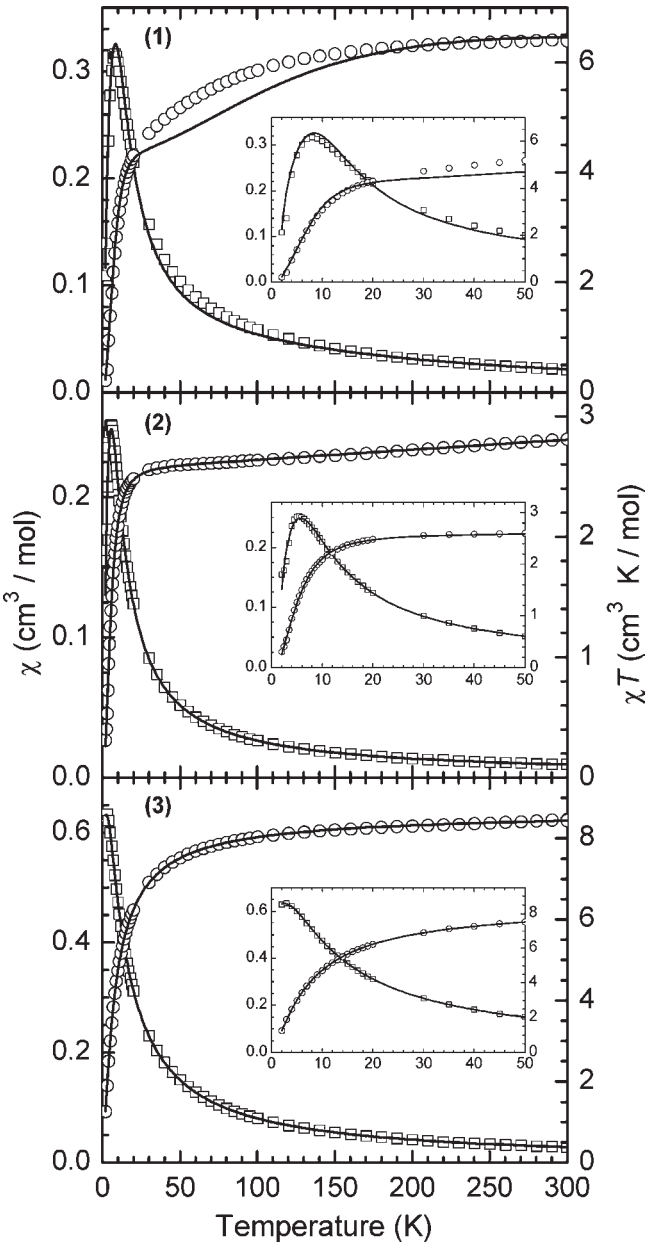

Figure 5. Temperature dependences of the low-field, $B = 0.1$ T, dc susceptibility, $\chi = M/B$, and product χT for **1**−**3**. All χ values are in units of cm^3/mol of dimer (M_2). The inset shows an expanded view at low temperature. In each panel, the data are represented by the symbols and the solid lines are the results of fitting. See the text for a description and Table 3 for the values of the fitting parameters.

a temperature-independent background, χ_0, that may arise from unsubtracted diamagnetic contributions. Taken together, these contributions can be written as

$$\chi(T) = \frac{\chi_{\text{dimer}}}{1 - \dfrac{2zJ'}{Ng^2\mu_B{}^2}\chi_{\text{dimer}}} + \rho\frac{2Ng^2\mu_B{}^2S(S+1)}{3k_BT} + \chi_0 \quad (3)$$

Using this expression, the results for **2**, where $S = 1$ because of the $^6A_{1g}$ state of Ni^{II}, and **3**, where $S = {}^5/_2$ because of the $^3A_{2g}$ state of Mn^{II}, were reasonably reproduced (Figure 5) with the values of the parameters listed in Table 3. On the other hand, the fits did not adequately reproduce the results of **1**, where $S = {}^3/_2$ because of the $^4T_{1g}$ state of Co^{II}; see the SI for details. Indeed, under these conditions and because of the finite spin−orbit coupling, the effective magnetic moment is expected to possess a significant temperature dependence that can be modeled by a parameter A if the spin−orbit coupling, λ, is known.[13,18] Taking the free-ion value of $\lambda = -(\xi/3) = -(515/3)\ \text{cm}^{-1} = -172\ \text{cm}^{-1}$,[13,18] the results of the fit, whose details are described in the SI, using the resulting parameters listed in Table 3 are given in Figure 5, where the data for **1** are still not well fit. Finally, for completeness, zero-field splitting was considered during fitting of the data for **2**,[19,20] and the corresponding parameter D was found to be small; see the SI for details.

Table 3. Parameters and Values Obtained from Analysis of the Magnetic Data[a]

	1	2	3
	$S = {}^3/_2$	$S = 1$	$S = {}^5/_2$
g	1.91[b]	2.26	1.98
	2.60[c]		
J	−5.3	−5.8	−1.1
zJ'	2.4	1.6	−0.33
ρ	0.02	0.02	0.003
χ_0	-1×10^{-4}	8×10^{-4}	2×10^{-4}
A	1.34		
$B_{\text{sat}}(T)$ (observed)	2.15 ± 0.05	3.2 ± 0.2	< 1.1
$B_{\text{sat}}(T)$ (expected, eq 4)	4.2	3.8	0.8

[a] Each fit was performed over the entire range of the data. All J and zJ' values are stated in units of K, and all χ_0 values are in units of cm^3/mol of dimer (M_2). [b] Calculated from eq S3 in the SI at $T = 2$ K. [c] Calculated from eq S3 in the SI at $T = 300$ K.

The results listed in Table 3 indicate that the interactions dominating the dimers are antiferromagnetic in nature. Ideally, the mean-field treatment used to generate eq 3 can be considered as an adequate approximation when the intradimer interactions are significantly stronger than the interdimer ones, and this limit is met for each compound studied herein, albeit not significantly so. In other words, more complex modeling of the materials is apparently needed, but these attempts should be guided by additional microscopic information, as might be obtained by inelastic neutron scattering studies, about the magnetic interaction network, and these steps are beyond the scope of the present work. Nevertheless, it is interesting that the interdimer interactions for **1** and **2** appear to possess a ferromagnetic tendency, and this outcome will be discussed later in this section.

Magnetic Properties: High Magnetic Field. The magnetic field dependences of the isothermal magnetization of **1**−**3** at $T = 2$ K are shown in Figure 6. The tendency to achieve saturation magnetization, arising from a field-induced fully polarized state, is clearly seen in **1** and **2** but only weakly reflected in the data of **3**. These observations are completely consistent with the interaction parameters extracted from the analysis of the low-field data (Table 3). In order to explore the transition from antiferromagnetic dimers to fully polarized spins, the $T \rightarrow 0$ limit ($T \ll J$) must be achieved in high magnetic fields, and these conditions were achieved with the instruments operated by the NHMFL-Gainesville (Figure 7). As discussed in detail in

(18) Figgis, B. N.; Hitchman, M. A. *Ligand Field Theory and Its Applications*; Wiley-VCH: New York, 2000.
(19) Ginsberg, A. P.; Martin, R. L.; Brookes, R. W.; Sherwood, R. C. *Inorg. Chem.* **1972**, *11*, 2884.
(20) Schlueter, J. A.; Manson, J. L.; Geiser, U. *Inorg. Chem.* **2005**, *44*, 3194.

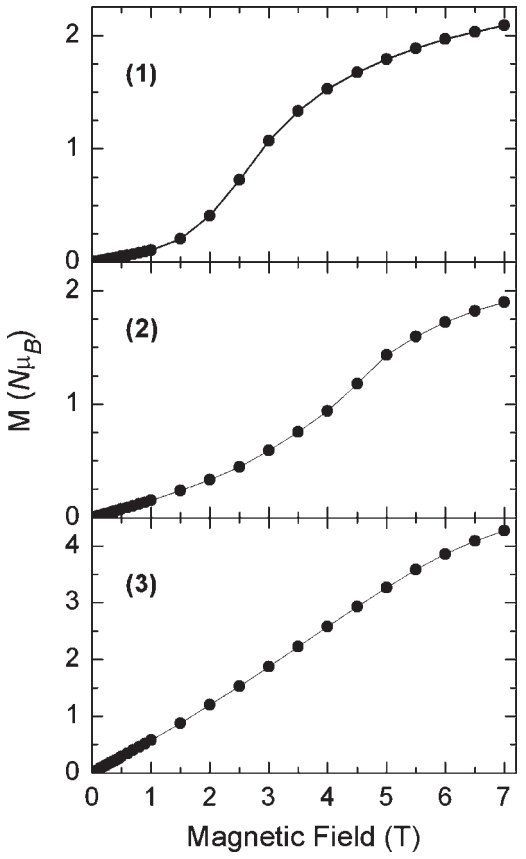

Figure 6. Magnetic field dependences of the isothermal (T = 2 K) magnetization, in units of $N\mu_B$, where N is Avogadro's number for atoms per mole of metal ion (i.e., not per dimer), for **1**−**3**. The solid lines are guides for the eyes.

the SI, the complexity of the experimental configurations did not allow for an independent measurement of the magnetic response of the background. However, if one assumes that the background is essentially temperature-independent at the lowest temperatures, then temperature-dependent features can be identified with **1** and **2** (Figure 7). These features are associated with the field-induced transition from the antiferromagnetically coupled dimer state to the spin-polarized state, which is expected to be steplike in the $T \rightarrow 0$ limit at a saturation field B_{sat} given by

$$g\mu_B B_{sat} = k_B J \quad (4)$$

The observed results and expected values, based on eq 4, are tabulated in Table 3. It is important to note that, in the presence of interdimer interactions, the simple prediction of eq 4 can be expected to be shifted to higher or lower fields, depending on the sign of the mean-field interactions. In fact, the magnetic parameters for each material are consistent with this tendency.

The low-temperature, high-field response of **3** was observed to be strongly hysteretic with a clear temperature dependence to the effect (Figure 7). Our interpretation of these results is that the sample, because of its rodlike geometry, was not completely immobilized in the sample holder. As a consequence, when the saturation magnetic field was achieved, the samples were able to physically align themselves with the applied field. Thermal

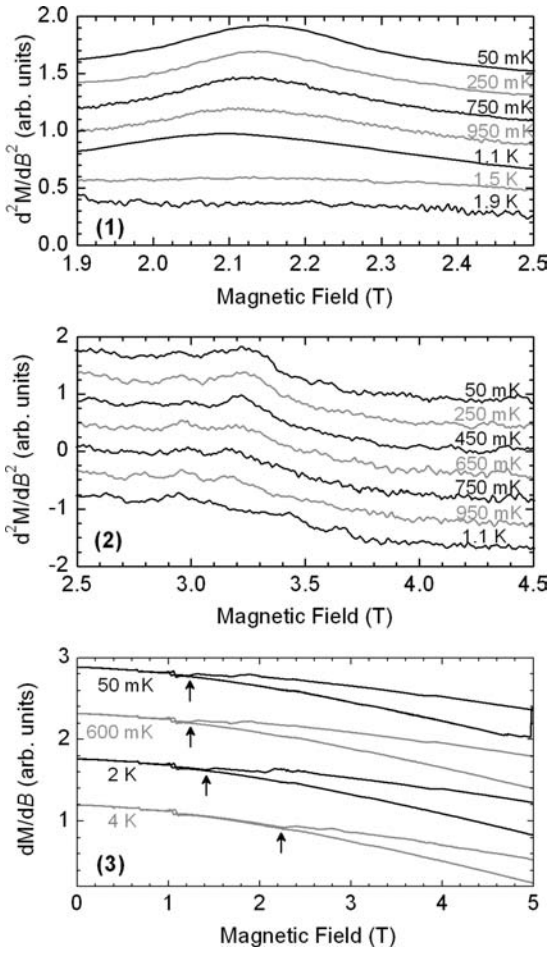

Figure 7. Isothermal ac response (dM/dB) or its derivative (d^2M/dB^2) as a function of the applied magnetic field for **1**−**3**. The temperatures are indicated on the plots, and the solid lines are 11-point averages of a dense set of data that were acquired while sweeping the field up or down spanning 0−10 T. For **3**, the arrows denote the lowest field below which the hysteresis is absent. See the text and the SI for a full discussion and expanded plots.

fluctuations at higher temperatures caused this alignment to move to higher fields, and this response is analogous to the thermal broadening of the transition seen in Figure 6. Ultimately, these results only allow us to place an upper bound on B_{sat} for **3** (Table 3).

Summary

The syntheses and structures of four isostructural metal monophosphonates with the formulas $M\{(2\text{-}C_5H_4NO)CH_2\text{-}PO_3\}(H_2O)_2$, where M = Co (**1**), Ni (**2**), Mn (**3**), and Cd (**4**), are reported. These compounds show a double-chain structure, with the $M_2(\mu\text{-}O)_2$ dimers connected by O−P−O bridges. Standard magnetic studies employing commercial SQUID magnetometers, combined with more specialized ac susceptibility studies at low temperatures (down to 50 mK) and in high magnetic fields (up to 10 T), allowed the dominant magnetic interactions to be identified as *nn* antiferromagnetic superexchange, leading to magnetic dimer units for **1**−**3**. A mean-field treatment of the interdimer interactions suggests that the presence of these kinds of interactions is non-negligible, but further characterization of these aspects requires microscopic magnetic studies that are beyond the scope of the present work.

Acknowledgment. This work was supported, in part, by NSFC (Grant 20631030), the National Basic Research Program of China (Grants 2007CB925102 and 2010CB923402), NSF of Jiangsu Province (Grant BK2009009), NSFC for Creative Research Group (Grant 20721002), the U.S. National Science Foundation via Grant DMR-0701400 (M.W.M.), and the National High Magnetic Field Laboratory by a cooperative agreement connecting Grant DMR-0654118 and the State of Florida. We thank Prof. You Song and Dr. Tian-Wei Wang for magnetic measurements made, in China, above 2 K, and Dr. Erik Čižmár for enlightening correspondence.

Supporting Information Available: (a) Details of the low-temperature, high-field measurements and additional data, (b) analysis of the high-temperature, low-field data that were acquired in Nanjing and in Gainesville, and (c) high-temperature ac susceptibility of **1**. This material is available free of charge via the Internet at http://pubs.acs.org.